Molecular Therapy
Oncolytics
Original Article

IRGM promotes melanoma cell survival through autophagy and is a promising prognostic biomarker for clinical application

Linlu Tian,[1,6] Hongxue Meng,[2,6] Xiao Dong,[1] Xinlei Li,[3] Zilin Shi,[1] Hulun Li,[4] Lie Zhang,[1] Yue Yang,[1] Ruijie Liu,[1] Chunying Pei,[1] Bo Li,[1] Hongwei Xu,[1] and Rui Li[5]

[1]Department of Immunology, Heilongjiang Provincial Key Laboratory for Infection and Immunity, Harbin Medical University, Harbin 150081, China; [2]Department of Pathology, Harbin Medical University Cancer Hospital, Harbin 150081, China; [3]Department of Anatomy, Harbin Medical University, Harbin 150081, China; [4]Department of Neurobiology, Harbin Medical University, Harbin 150081, China; [5]Department of Neurology and Center for Neuroinflammation and Experimental Therapeutics, University of Pennsylvania, Philadelphia, PA 19104, USA

Previously, we showed that mouse immunity-related guanosine triphosphatase (GTPase) family M protein 1 (Irgm1) promotes malignant melanoma progression by inducing cellular autophagy flux and metastasis. Human IRGM, a truncated protein functionally distinct from its mouse counterpart, has several splice isoforms. In this study, we analyzed the association of IRGM and human melanoma clinical prognosis and investigated the function of IRGM in human melanoma cells. Data from the training cohort (n = 144) showed that overexpression of IRGM is proportional to melanoma genesis and clinical stages in human tissue chips. A validation cohort (n = 78) further confirmed that IRGM is an independent risk factor promoting melanoma progression and is associated with poor survival of patients. Among IRGM isoforms, we found that IRGMb is responsible for such correlation. In addition, IRGM promoted melanoma cell survival through autophagy, both *in vitro* and *in vivo*. We further showed that the blockade of translocation of high-mobility group box 1 (HMGB1) from the nucleus to cytoplasm inhibits IRGM1-mediated cellular autophagy and reduces cell survival. IRGM functions as a positive regulator of melanoma progression through autophagy and may serve as a promising prognostic marker and therapeutic target.

INTRODUCTION

Melanoma is a malignant tumor with increasing annual incidence and range of onset areas. Gene mutations (such as those in BRAF and Akt), excessive ultraviolet radiation, and family hereditary history are the main causes of benign nevus progression into melanoma.[1,2] Despite the application of various strategies, including surgical resection, radiochemotherapy, and immunotherapy, in the clinic, patients experience low survival rates, rapid metastasis, and poorer prognosis with the existing treatments.[3–5] Autophagic flux is a cellular degradation process that facilitates cell metabolism and self-renewal under starvation by digesting the cell's own cytoplasm and recycling energy.[6,7] This process affects aging, neurodegeneration, myodegeneration, cancer development,[8–10] and immunity.[11,12] Research to date supports a role of autophagy in rescuing tumor cells from viability stress and immune escape through impairment of apoptosis.[13–15] The interferon (IFN)-inducible immune-related guanosine triphosphatase (GTPase) family M protein 1 (Irgm1) has been shown to be essential for regulating mouse melanoma tumorigenesis[16] and metastasis[17] through autophagy-dependent and -independent mechanisms. Human IRGM is different from mouse Irgm1, as it is a truncated protein and may not be induced by various IFNs.[18,19] Human IRGM has been shown to modulate human macrophage-related *Mycobacterium tuberculosis* elimination through activation of autophagy by coupling to the autophagy factor ATG16L1, a risk locus for Crohn's disease.[20] Irgm1/IRGM-mediated autophagy has been implicated in multiple disease contexts, including stroke and atherosclerosis.[10,21] IRGM has five splices in humans, including IRGMa, IRGMb, IRGMc, IRGMd, and IRGMe.[9] In this study, we would sought to explore the potential role of different IRGM splices in the contexts of melanoma.

Using two independent cohorts of melanoma patients and controls, we showed that IRGM, in particular IRGMb, is associated with melanoma genesis and progression. Functional experiments further revealed that IRGM is a crucial survival factor for melanoma. IRGM promotes melanoma cell survival through interacting with high motility group box 1 (HMGB1), which in turn promotes autophagy.

Received 20 July 2020; accepted 11 December 2020;
https://doi.org/10.1016/j.omto.2020.12.005.

[6]These authors contributed equally

Correspondence: Hongwei Xu, Department of Immunology, Heilongjiang Provincial Key Laboratory for Infection and Immunity, Harbin Medical University, 156 Baojian Road, Nangang District, Harbin, Heilongjiang Province 150081, China.
E-mail: hongwei56@hotmail.com
Correspondence: Rui Li, Department of Neurology and Center for Neuroinflammation and Experimental Therapeutics, University of Pennsylvania, 3450 Hamilton Walk, Philadelphia, PA 19104, USA.
E-mail: lirui158@pennmedicine.upenn.edu

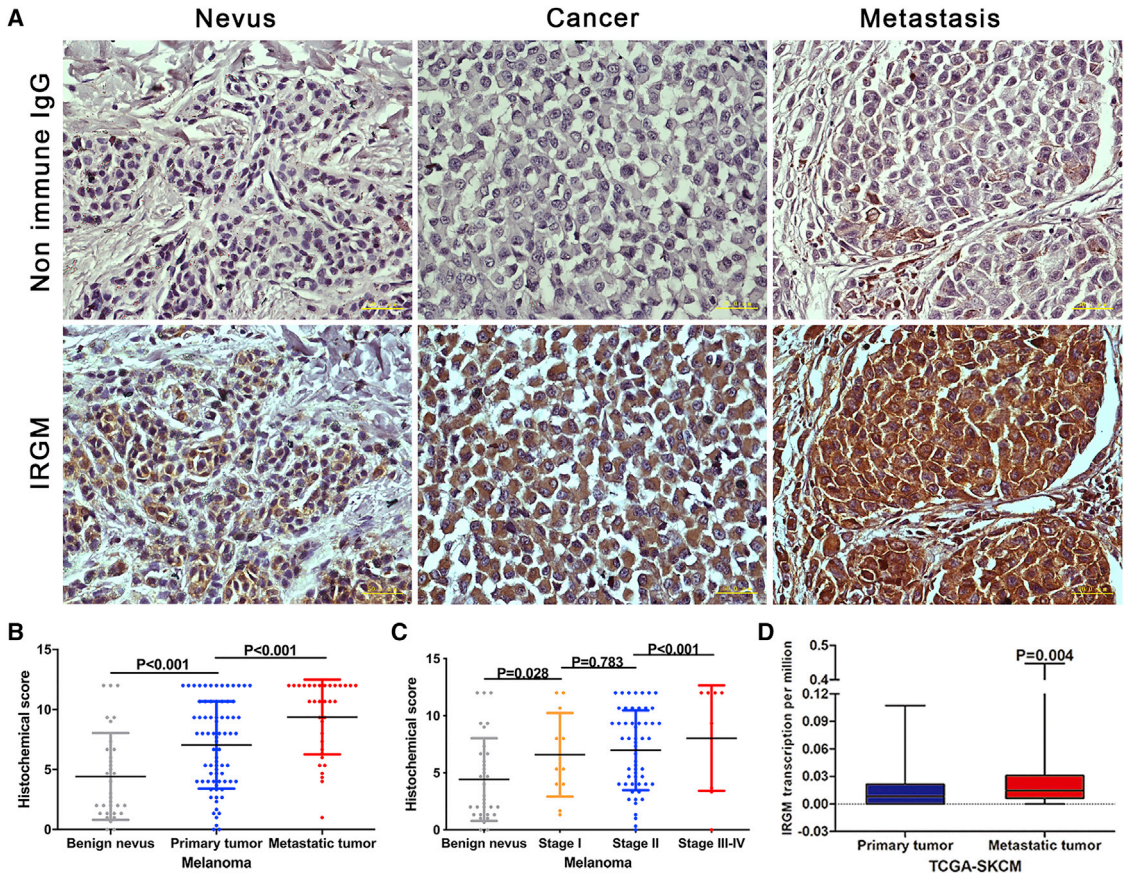

Figure 1. IRGM promotes melanoma genesis and metastasis

Tissue chips were used for assessing the relationship between IRGM expression and melanoma malignant progression. (A) IRGM expression was detected via IHC staining in benign nevus, primary melanoma, and metastatic tumor foci. (B) IHC scores. (C) Based on the clinical outcomes of tissue chips, IRGM levels were compared between benign nevus and each stage of primary melanoma. (D) IRGM transcription levels (FRPM value) of patients were compared between primary and metastatic tumors. Data are presented as means ± SD (U test).

RESULTS

IRGM expression is associated with melanoma progression

To ascertain the potential relationship between IRGM and melanoma progression, we initially applied immunohistochemistry (IHC) staining in human tissue chips. With the exception of 56 cases displaying severe melanin diffusion, IHC scores from 144 cases were evaluated, including patient benign nevus, primary, and metastatic melanoma tissues (Table S1). Expression of IRGM was obviously higher in primary melanoma tissues (IHC score: 7.42 ± 3.73, 95% CI [6.49, 8.36]) than that of human benign nevus (IHC score: 4.41 ± 3.62, 95% CI [3.13, 5.69], $p < 0.001$) and lower than metastatic melanoma tissues (IHC score: 9.37 ± 3.11, 95% CI [8.29, 10.46], $p < 0.001$) (Figures 1A and 1B; Table S1). Next, we defined the expression standards based on IHC scores (low expression, 0–6; high expression, 7–12), and patient counts with differential IRGM expression patterns were obtained. We recorded a higher percentage of patients displaying high IRGM1 expression in primary melanoma (52.6%) than benign nevus (21.2%) groups and a lower percentage than in metastatic melanoma (73.5%), and there were significant differences between groups (benign nevus versus primary melanoma, $p = 0.001$; primary melanoma versus metastatic melanoma, $p = 0.027$) (Table S2). Furthermore, increased expression of IRGM was proportional to malignant melanoma stages in human tissue chips, in particular, from the benign nevus to stage I ($p = 0.028$) and stage II to stages III–IV ($p < 0.001$) (Table S1; Figure 1C). Simultaneously, a search of 469 melanoma cases in The Cancer Genome Atlas (TCGA) database disclosed that compared with primary melanoma (101 cases; fragments per kilobase of transcript per million mapped reads [FPKM] value: 0.014 ± 0.019, 95% CI [0.010, 0.018]), IRGM mRNA levels in metastatic melanoma (368 cases; FPKM value: 0.028 ± 0.048, 95% CI [0.023, 0.033]) were markedly higher ($p = 0.004$, Figure 1D). These preliminary data clearly demonstrated a stimulatory effect of IRGM on melanoma progression and metastasis.

Increased IRGM transcript and protein expression during melanoma progression

Due to the limitations of human tissue chips, including variable treatments, small sizes, and melanin diffusion, the precise relationship

between IRGM and melanoma progression is currently unclear. To resolve this issue, 87 primary melanoma and paracancerous paraffin blocks from 78 patients were included from the Harbin Medical University Cancer Hospital for setting up a validation cohort. In this study, IRGM was detected from transcript and protein levels separately. Compared with paracancerous tissues (mRNA fold change: 1.26 ± 1.42, 95% CI [0.07, 2.44]), the transcripts of IRGM in melanoma (mRNA fold change: 5.42 ± 7.00, 95% CI [3.80, 7.04]) were obviously increased, and with significant differences ($p < 0.001$) (Table S3; Figure 2A). Additionally, IRGM presented a significant transcriptional increase in association with higher melanoma stages (Table S3; Figure 2B). Similar results were obtained from IHC analyses, showing higher expression of IRGM in melanoma (IHC score: 1.60 ± 3.37, 95% CI [3.24, 4.76]) than paracancerous tissues (IHC score: 4.00 ± 3.66, 95% CI [−0.81, 4.01]) ($p = 0.014$). We further observed a higher number of IRGM-positive cells and more intense staining in cancerous tissues with advancing melanoma stages (Table S3; Figures 2C–2E). Our collective data suggested that IRGM mRNA and protein levels were enhanced during the course of malignant progression.

To further test the association between IRGM and survival of patients, detailed clinical information, follow-up, and overall survival of the 78 cases in the validation cohort were collected and recorded (Table 1). Kaplan-Meier survival analysis showed that patients with IRGM extensive expression underwent shorter overall survival (IRGM high [33.78%] versus low [66.22%]: 921.65 ± 115.84, 95% CI [694.60, 1,148.70] versus 1,391.52 ± 96.53, 95% CI [1,202.33, 1,580.71], $p = 0.008$), and the similar trend was found on IRGM transcript levels (IRGM high [50.00%] versus low [50.00%]: 890.90 ± 102.13, 95% CI [690.72, 1,091.08] versus 1,476.08 ± 104.44, 95% CI [1,271.37, 1,680.79], $p = 0.002$) (Table 1; Figures 2F and 2G) The statistical results suggested that a high level of IRGM was associated with a decline in survival of melanoma patients.

IRGM is an independent risk factor for melanoma prognosis

Based on previous reports, sex, age, smoking, alcohol use, tumor history, and tumor family history may be classical or potential routine risk factors regulating malignant melanoma prognosis.[22–27] Kaplan-Meier survival and hazard ratio (HR) value analysis were first used to evaluate the significant routine risk factors in this validation cohort separately. Comprehensive data suggested that smoking (yes [18.92%] versus no [81.08%]: 779.13 ± 113.46 versus 1,348.80 ± 94.13, $p = 0.049$; HR = 2.667, $p = 0.012$), alcohol use (yes [10.46%] versus no [90.54%]: 658.00 ± 198.64 versus 1,315.84 ± 88.73, $p = 0.011$; HR = 3.261, $p = 0.010$), and tumor family history (yes [2.70%] versus no [97.30%]: 574.93 ± 289.5 versus 1,266.43 ± 86.72, $p = 0.016$; HR = 4.981, $p = 0.031$) were candidates that affected mortality risk and survival of melanoma patients within the validation cohort, with significant differences in both Kaplan-Meier survival and HR analysis (Table 1; Figure 2H). To further determine whether IRGM (transcript: HR = 3.217, 95% CI [1.454, 7.115], $p = 0.004$; expression: HR = 2.525, 95% CI [1.114, 5.726], $p = 0.027$) was an independent risk factor excluded from other clinical candidates that were associated with melanoma prognosis, a Cox proportional hazards model was established. Data revealed that when IRGM was considered as a dominant variant, it could ignore cooperative variants (smoking, alcohol use, and tumor family history) and showed an independent risk effect on patients' mortality and prognosis (transcription: HR = 2.087, $p = 0.016$; expression: HR = 2.609, $p = 0.031$, Table 2). Combined these clinical data, we concluded that the high level of IRGM promoted melanoma progression clearly and was associated with patients' prognosis independently.

IRGMb is the crucial splice isoform that promotes melanoma genesis

Singh et al.[9] showed that different splice isoforms of IRGM (IRGMa, IRGMb, IRGMc, IRGMd, and IRGMe) exert variable effects on cellular autophagy and function. In view of this finding, we examined the transcript levels of these splice isoforms in melanoma. Notably, compared with paracancerous tissues, IRGMb, IRGMc, and IRGMd levels were higher while those of IRGMa and IRGMe were lower (Figures 3A–3E; Table S4). Calculation of the ratios of transcript levels of each IRGM isoforms in melanoma to paracancerous tissues revealed that IRGMc and IRGMd displayed lower mRNA fold changes than did IRGMb, and with a significant difference ($p < 0.001$, Figure 3F). Furthermore, Kaplan-Meier survival and HR value analysis suggested that compared with other IRGM isoforms, patients with high level of IRGMb suffered shorter overall survival and a higher HR value (IRGM high versus low: 970.91 ± 102.35, 95% CI [770.31, 1,171.51] versus 1,510.97 ± 110.27, 95% CI [1,294.85, 1,727.10], $p = 0.004$; HR = 3.108, 95% CI [1.375, 7.024], $p = 0.006$) (Figures 3G–3L; Table 3). Data from Cox regression analysis also supported that IRGMb was an independent risk factor for melanoma prognosis, ignoring cooperative variants (smoking, alcohol use, and tumor family history) (Table 4). These results highlighted that IRGMb was considered as the potentially important isoform in melanoma progression.

IRGM induces melanoma cell survival *in vivo* and *in vitro*

Clinical data suggest that IRGM plays a positive role in melanoma progression. To further establish the effects and mechanisms of action of IRGM, experiments were performed to examine its influence on melanoma *in vivo* and *in vitro*. After knockdown of IRGM with short hairpin RNA (shRNA) in human A375 melanoma cells (Figure 4A), cell survival and apoptosis outcomes were measured with the Cell Counting Kit-8 (CCK8) assay and propidium iodide (PI)/annexin V staining. Compared with non-treated and control shRNA-treated cells, knockdown led to markedly reduced cell viability (Figure 4B) and increased apoptosis (Figures 4C and 4D). To validate this finding *in vivo*, we established tumor-bearing BALB/c nude mouse models via subcutaneous or intravenous injection with A375 melanoma cells transfected with control or IRGM shRNA. Compared with the control groups, IRGM deletion led to significantly prolonged mouse survival (Figure 4E) as well as decreased tumor sizes and weights (Figures 4F and 4G), supporting a stimulatory role of this molecule in human melanoma progression.

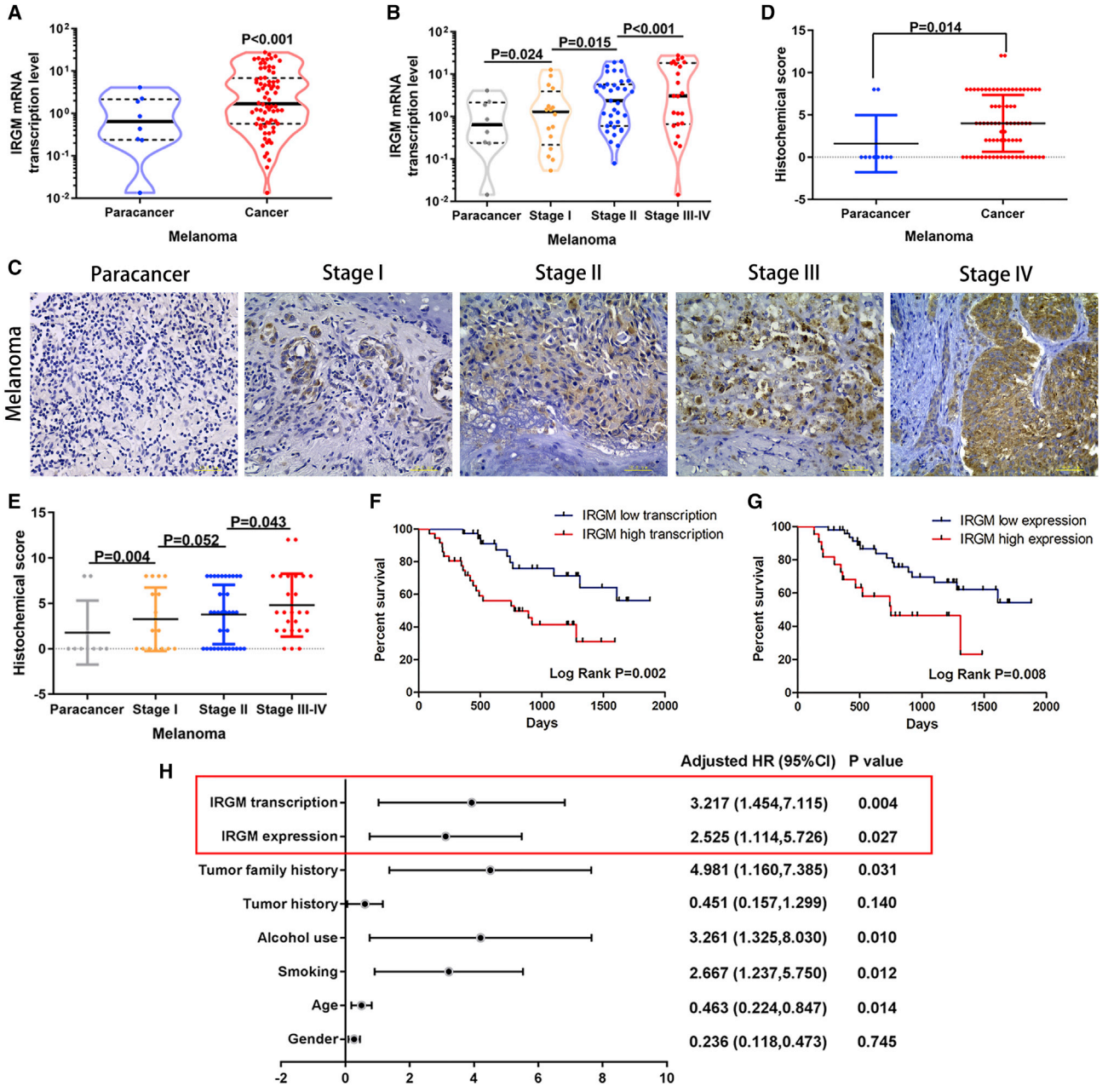

Figure 2. IRGM transcript and protein levels increase with melanoma progression

The relationship between IRGM and melanoma progression was validated using cancerous and paracancerous tissues embedded in paraffin from 78 melanoma cases. IRGM transcription was detected in tissue RNA from paraffin blocks. (A and B) IRGM transcript levels were compared between paracancerous tissue and (A) total cancerous tissue or (B) cancerous tissue from each stage. (C) Data from IHC staining. (D and E) IHC scores were compared between paracancerous tissue and (D) total cancerous tissue or (E) cancerous tissue from each stage. (F) Based on the median of transcript levels, patients were divided into IRGM high or IRGM low transcription groups, and overall survival was compared between these two groups. (G) Overall survival was compared between IRGM high or IRGM low expression groups (IRGM low expression group, IHC score of 0–6; IRGM high expression group, IHC score of 7–12). Data are presented as means ± SD (U test). (H) HR values were used to evaluate the effect of different clinical outcomes on patients' survival.

Table 1. Kaplan-Meier survival analysis of clinical outcomes from 78 melanoma patients

Clinical outcomes	Patients (%)	Survival ± SD (95% CI)	p value (log rank)
Sex			
Male	39 (52.70)	1,097.58 ± 118.30 (865.72, 1,329.43)	0.063
Female	35 (47.30)	1,315.28 ± 99.77 (1,119.734, 1,510.829)	
Age			
<60	43 (58.11)	1,277.58 ± 116.32 (1,049.45, 1,505.58)	0.676
>60	31 (41.89)	1,146.05 ± 108.62 (933.16, 1,358.93)	
Smoking			
Yes	14 (18.92)	779.13 ± 113.46 (556.75, 1,001.52)	0.049
No	60 (81.08)	1,348.80 ± 94.13 (1,164.30, 1,533.31)	
Alcohol use			
Yes	7 (10.46)	658.00 ± 198.64 (269.01, 1,046.99)	0.011
No	67 (90.54)	1,315.84 ± 88.73 (1,141.92, 1,489.76)	
Tumor history			
Yes	16 (21.62)	1,370.40 ± 144.49 (1,087.20, 1,653.60)	0.130
No	58 (78.38)	1,160.44 ± 97.62 (969.11, 1,351.77)	
Tumor family history			
Yes	2 (2.70)	460.50 ± 289.50 (574.93, 1,027.92)	0.016
No	72 (97.30)	1,266.43 ± 86.72 (1,096.47, 1,436.40)	
IRGM expression			
High	25 (33.78)	921.65 ± 115.84 (694.602, 1,148.70)	0.008
Low	49 (66.22)	1,391.52 ± 96.53 (1,202.33, 1,580.71)	
IRGM transcription			
High	37 (50.00)	890.90 ± 102.13 (690.72, 1,091.08)	0.002
Low	37 (50.00)	1,476.08 ± 104.44 (1,271.37, 1,680.79)	

78 melanoma cases were randomly enrolled to evaluate the influence of IRGM on melanoma progression. Kaplan-Meier survival analysis of clinical outcomes from 78 melanoma patients was used. For IRGM IHC staining, a score of 0–6 was defined as IRGM low expression, and a score of 7–12 was defined as IRGM high expression. For IRGM transcription, based on the median of mRNA fold change, patients were divided into IRGM high or low transcription groups.

Table 2. Cox proportional hazards model: IRGM expression (transcription) test

			95.0% CI for HR	
Variables	Significance	HR	Lower	Upper
IRGM	0.031 (0.016)	2.609 (2.087)	1.090 (0.901)	6.424 (4.835)
Alcohol use	0.055 (0.093)			
Smoking	0.112 (0.053)			
Tumor family history	0.647 (0.354)			

A Cox proportional hazards model was established to verify the independent effect of IRGM on human melanoma. IRGM (transcript and expression) is presented as a dominant factor; alcohol use, smoking, and tumor family history are presented as cooperative factors.

IRGM-mediated rescue of human melanoma cells is dependent on HMGB1-related autophagy

IRGM is a critical autophagy-related protein that regulates multiple diseases.[20,28–30] Previous studies have demonstrated that mouse Irgm1 regulates melanoma survival through binding the autophagy factor Bif-1 and further promoting autophagic flux.[16] Accordingly, we examined the hypothesis that IRGM may similarly regulate melanoma through an autophagic pathway although the protein structures and molecular weights of the human and mouse homologs are distinct.[18] By transmission electron microscopic study, we found that knockdown of IRGM decreased starvation-induced autophagosomes in A375 and A875 melanoma cells (Figure 5A; Figure S1A). Consistent with the transmission electron microscopic results, IRGM knockdown suppressed lipidation of LC3 and degradation of SQSTM1 upon nutrition-deprived medium culture for an additional 6 and 12 h, the indicator proteins of autophagy (Figure 5B; Figure S1B). A finding further supported by TUNEL (terminal deoxynucleotidyltransferase-mediated deoxyuridine triphosphate [dUTP] nick end labeling) staining data. Melanoma cells treated with control or IRGM shRNA displayed similar apoptosis levels after stimulation with 3-methyladenine (3-MA), an autophagy inhibitor (Figure 5C; Z-VAD-fmk, a pan apoptosis inhibitor, was used as the positive control).

HMGB1 is considered an autophagy-related protein that enhances autophagy upon accumulation in the cytoplasm.[31,32] We observed no differential expression of HMGB1 in A375 total cell lysates, but translocation to the cytoplasm was evident when autophagy was induced by starvation with a low-glucose cell culture (Figure S2A). In the presence of erythropoietin (EP), which suppressed translocation of HMGB1 from the cellular nucleus to cytoplasm, autophagy of A375 melanoma cells was impaired and apoptosis was enhanced (Figures S2B–S2D). Based on this finding, we speculated that IRGM binds HMGB1 to induce autophagy. Data from co-immunoprecipitation (coIP) and immunofluorescence experiments supported this hypothesis. IRGM formed a complex with HMGB1 in the cytoplasm, especially after starvation for 6 h (Figures 5D and 5E). Moreover, upon inhibition of HMGB1 translocation, formation of the IRGM-HMGB1 complex was markedly reduced (Figure 5F). The proliferative ability of control- or IRGM shRNA-treated A375 cells was

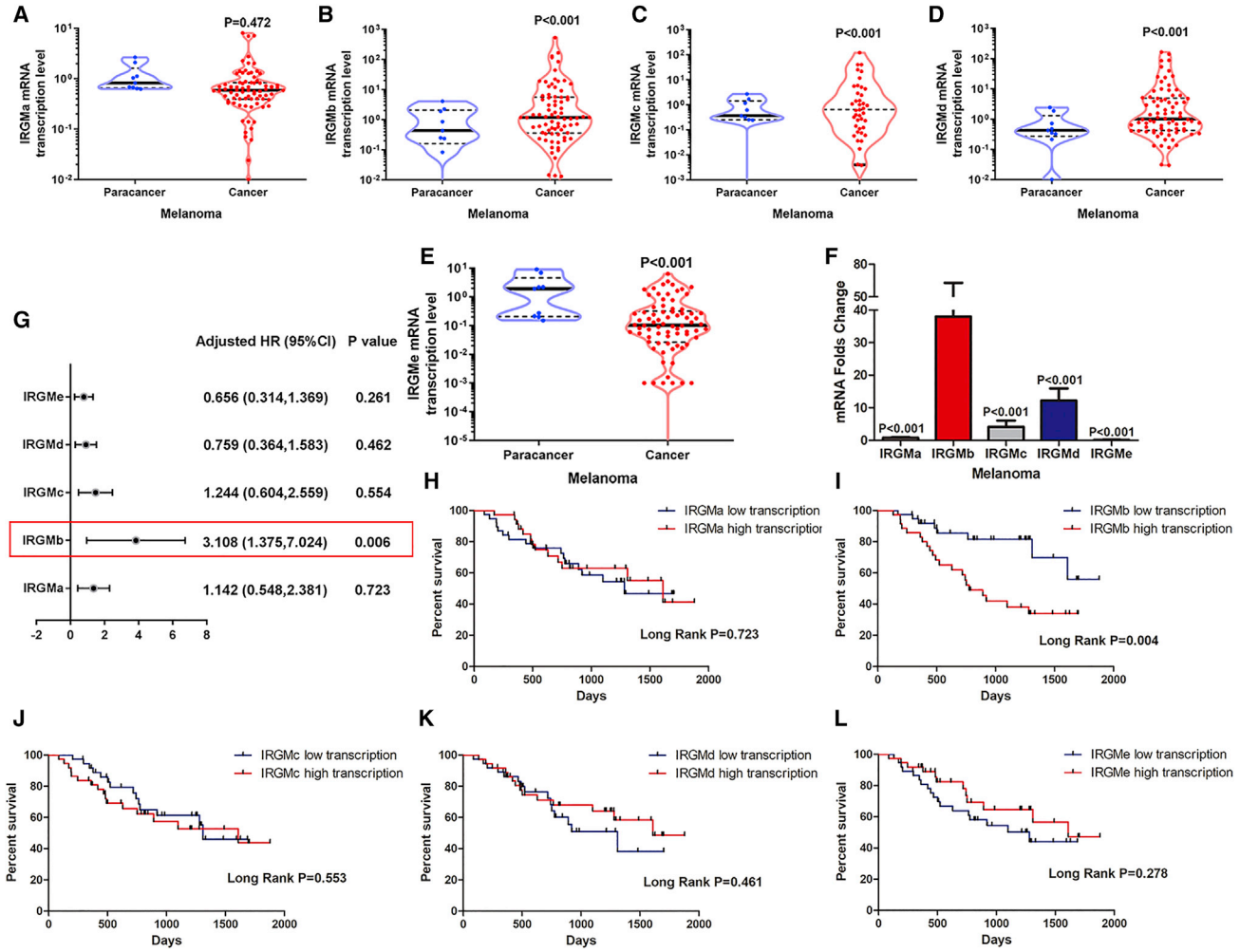

Figure 3. IRGMb is the crucial splice isoform for regulation of melanoma

(A–E) Transcript levels of various IRGM splice isoforms were detected in paracancerous and cancerous tissues of 78 melanoma cases, including (A) IRGMa, (B) IRGMb, (C) IRGMc, (D) IRGMd, and (E) IRGMe. (F) Fold changes of IRGM isoform mRNA levels (cancerous/paracancerous tissue). (G) HR values were used to evaluate the effect of different IRGM splice isoforms on patients' survival. (H–L) Based on the median of transcript levels of various IRGM splice isoforms, patients were divided into high or low transcription groups, and overall survival was compared between these two groups for different IRGM splice isoforms, including (H) IRGMa, (I) IRGMb, (J) IRGMc, (K) IRGMd, and (L) IRGMe. Data are shown as means ± SD (U test).

additionally determined. Compared with IRGM shRNA-treated cells, those treated with control shRNA displayed reduced viability to a significant extent after stimulation with EP or chloroquine (CQ), an autophagy inhibitor (Figure 5G). Our collective results demonstrated that IRGM promoted melanoma cell survival via autophagy through interactions with HMGB1.

IRGM prolongs the autophagic flux in a manner dependent on recruitment of Beclin1 by HMGB1

The HMGB1-Beclin1 complex is the classical mediator of cellular autophagy.[31,33] CoIP and immunofluorescence assays revealed that IRGM formed complexes with HMGB1 and Beclin1 (Figures S3A and S3B). In accordance with cytoplasmic immunoprecipitation, the IRGM-HMGB1 complex accumulation reached a peak during starvation at the 6 h time point in A375 total cell lysates, similar to the IRGM-Beclin1 complex. Nevertheless, the levels of both complexes decreased after long-term starvation (Figure 5D; Figure S1A). We speculate that melanoma cells might preform "non-health" and HMGB1 release from cells. Interestingly, application of EP to inhibit HMGB1 translocation to the cytoplasm led to breakdown of the IRGM-HMGB1 complex (Figure 5F). Our data suggested that HMGB1 was an intermediate that aided in the recruitment of Beclin1 by IRGM and further prolonged the autophagic flux.

DISCUSSION

Studies on immune-related GTPase Irgm1/IRGM have shown genetic linkages with Crohn's disease, inflammation diseases, and autoimmune diseases in different populations worldwide.[28,34–36] Some

Table 3. Kaplan-Meier survival analysis of IRGM splice isoforms from 78 melanoma patients

IRGM splice isoforms (transcription)	Survival ± SD (95% CI)	p value (log rank)
IRGMa		
High	1,144.39 ± 105.04 (938.51, 1,350.27)	0.723
Low	1,284.37 ± 122.97 (1,043.35, 1,525.38)	
IRGMb		
High	970.91 ± 102.35 (770.31, 1,171.51)	0.004
Low	1,510.97 ± 110.27 (1,294.85, 1,727.10)	
IRGMc		
High	1,197.02 ± 98.52 (1,003.92, 1,390.12)	0.553
Low	1,021.27 ± 125.63 (955.02, 1,447.51)	
IRGMd		
High	1,321.69 ± 116.22 (1,093.89, 1,449.48)	0.461
Low	1,101.74 ± 109.72 (886.69, 1,316.79)	
IRGMe		
High	1,331.50 ± 122.31 (1,091.78, 1,571.23)	0.278
Low	1,077.05 ± 103.69 (873.82, 1,280.29)	

Kaplan-Meier survival analysis of various IRGM splice isoforms from 78 melanoma patients. Results are based on the median of mRNA fold change; patients were divided into IRGMa–IRGMe high or low transcription groups.

Table 4. Cox proportional hazards model: IRGMb transcription test

			95.0% CI for HR	
Variables	Significance	HR	Lower	Upper
IRGMb	0.002	3.724	1.638	8.468
Alcohol use	0.132			
Smoking	0.804			
Tumor family history	0.349			

A Cox proportional hazards model was established to verify the independent effect of IRGMb on human melanoma. The IRGMb transcript is presented as a dominant factor; alcohol use, smoking, and tumor family history are presented as cooperative factors.

research has also strongly suggested that Irgm1/IRGM are potential direct targets participating in autophagy flux and further regulate various disease.[28,37] Although our previous research demonstrated that Irgm1 promotes melanoma cell survival[16] and metastasis,[17] there is not still enough evidence to reveal the association of IRGM and melanoma. In this research, we took a systematic approach to define the extent of IRGM level that is prognostically relevant from clinical cohorts in *in vitro* and *in vivo* experiments.

Data obtained from clinical training and validation cohorts disclosed a positive relationship between IRGM extensive expression and melanoma progression, with significant differences in transcript and protein levels among paracancerous tissue (benign nevus), primary melanoma, and metastatic melanoma, or different stages of primary melanoma. Notably, IRGM1 levels (transcript and expression) increased with progressive stages of malignant melanoma and obviously shortened patients' overall survival, with significant differences. Consistent with previous research, smoking, alcohol use, and tumor family history showed a clear relationship to melanoma patients' poor survival and prognosis in this validation cohort. In this study, to prove the independence of IRGM on melanoma progression and ignore these routine risk factors, a Cox regression model was set up. Data suggested that IRGM was the independent risk factor, and the mortality risk of patients with a high IRGM level was around 2-fold that of patients with a low IRGM level.

An earlier study by Singh et al.[9] reported various splice isoforms of IRGM (including IRGMa, IRGMb, IRGMc, IRGMd, and IRGMe) with different functions. In this study, IRGMb acted as a unique isoform that was associated with patients' overall survival, and the changing trend was consistent with IRGM. Results from Cox regression analysis showed that IRGMb was an independent risk factor that was not affected by other potential candidates. Mortality risk of patients with a high IRGMb level was around 2-fold that of patients with a low IRGMb level.

Autophagy performs dual regulatory roles in tumor progression and metastasis. According to its physiological function, autophagy facilitates tumor cell survival during stress via energy circulation.[16,38,39] However, hypernomic autophagy is also reported to act against tumor progression by inducing autophagic cell death and inhibiting melanoma development.[40,41] In this study, the autophagy-related protein IRGM was characterized as a positive factor for melanoma survival through induction of autophagy. Co-assembly of IRGM with ULK1 and Beclin1 has been previously reported. During exposure to viral or microbial products, IRGM functions as a platform for assembling, stabilizing, and activating the core autophagic machinery.[20] Our data suggested that IRGM coupled with HMGB1 in the cytoplasm in melanoma cells to induce autophagy under nutrient-deprived culture conditions. In view of the finding that HMGB1-Beclin1 is the classical complex regulating autophagy in human cells,[32,33] co-assembly of IRGM, HMGB1, and Beclin1 was additionally examined. IRGM interacted with both HMGB1 and Beclin1, with accumulation of complexes after starvation for 6 h (Figure S3), indicating that IRGM combined with HMGB1 and Beclin1 to prolong autophagy in human cancer calls. Although IRGM appears to be a key factor involved in autophagic flux,[9,20] it may form different functional complexes during variable disease processes. We speculate that this may be due to discrepancies in IRGM states or structures and expression patterns of different IRGM splice isoforms, leading to diverse outcomes.

Previous studies by our group demonstrated that mouse Irgm1 promotes melanoma survival[16] and metastasis.[17] In the present study,

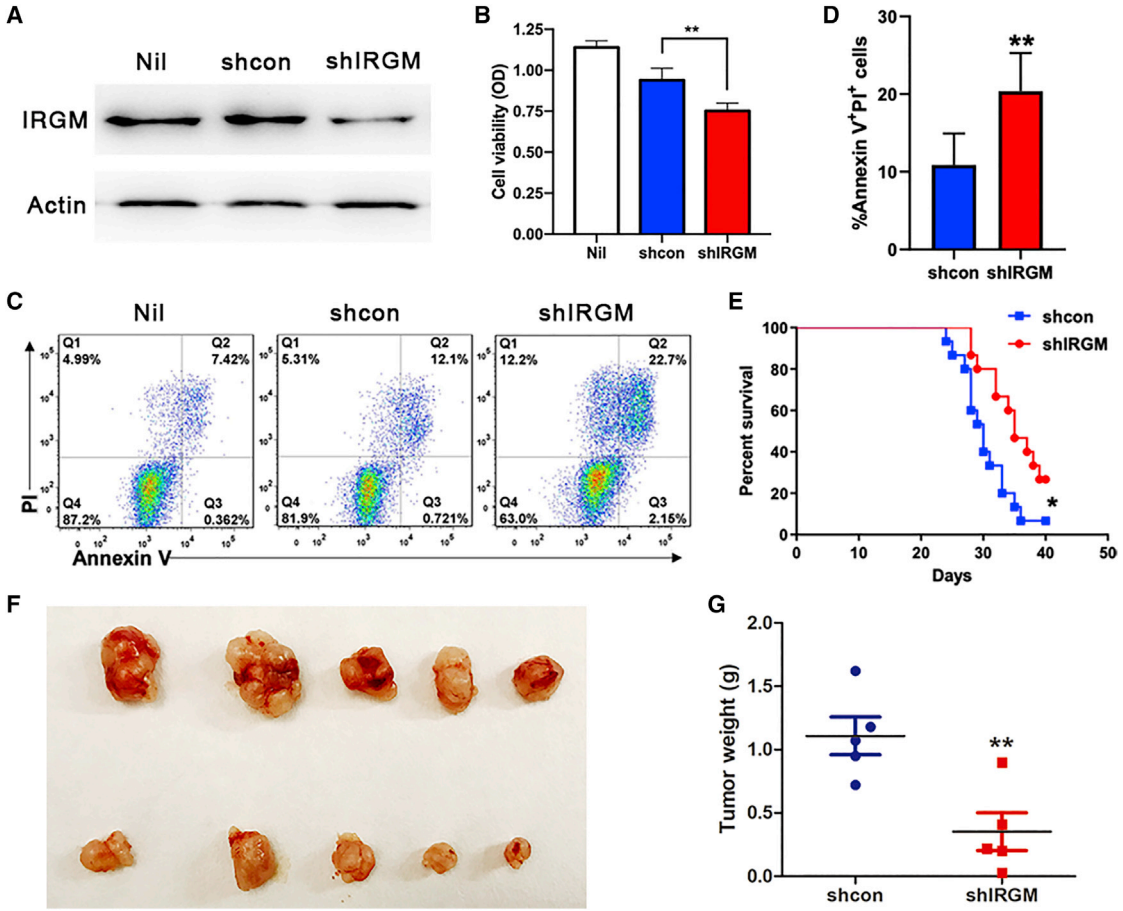

Figure 4. IRGM promotes melanoma cell survival *in vitro* and *in vivo*

(A) Western blot analysis of IRGM expression in A375 cells after transfection with control or IRGM shRNA. (B) A375 cells were transfected with control shRNA or IRGM shRNA and subjected to a CCK8 assay. (C and D) PI/annexin V staining for evaluation of A375 cell apoptosis after transfection with control shRNA or IRGM shRNA. (E) Control or IRGM shRNA-treated A375 cells (2×10^6) were injected into the tail vein of BALB/c nude mice and percentage survival recorded (combined survival data were from two independent experiments, six mice/group/experiment). Control shRNA- or IRGM shRNA-treated A375 cells (2×10^6) were additionally subcutaneously injected into BALB/c nude mice to establish melanoma-bearing mouse models. (F) Measurement of tumor growth after sacrifice of mice on day 30. (G) Tumor weights (two independent experiments were conducted for examination of tumor nodes, five mice/group/experiment). Data are presented as means ± SD (*$p < 0.05$, **$p < 0.01$, ***$p < 0.001$).

we confirmed that the truncated homolog can also effectively rescue human melanoma under nutrient deprivation conditions through enhancement of autophagy. Moreover, differential transcript and protein levels of IRGM were associated with tumorigenesis, metastasis, and even patients' survival, supporting the utility of this molecule as a promising biomarker and therapeutic target for melanoma.

MATERIALS AND METHODS

Melanoma tissue chips and patient samples

Human melanoma tissue chips were purchased from US Biomax (Me1004b, Me1004e; Alenabio, Xian, China). Each tissue chip contained 100 cases, including benign nevus, primary melanoma, and metastatic melanoma tissues. With the exception of 56 cases with severe melanin diffusion, the remaining 144 cases were used to detect IRGM expression.

Patient samples and follow-up

In total, 87 paraffin blocks from 78 melanoma patients were collected from Harbin Medical University Cancer Hospital, including 9 paracancerous and 78 cancerous tissues. All enrolled patients signed informed consent and received approval from the Ethics Committee of Harbin Medical University. The onset of patients was from July 2014 to September 2018, according to pathology reports and cases history, clinical information from 78 patients was collected, and further survival was recorded based on follow-up until September 2019.

IHC staining and scores

Embedded sections were subjected to antigen retrieval with citrate buffer (pH 6.0), incubated with mouse anti-human IRGM monoclonal antibody (Ab; 1G9; AbMart, Shanghai, China; 1:200), and

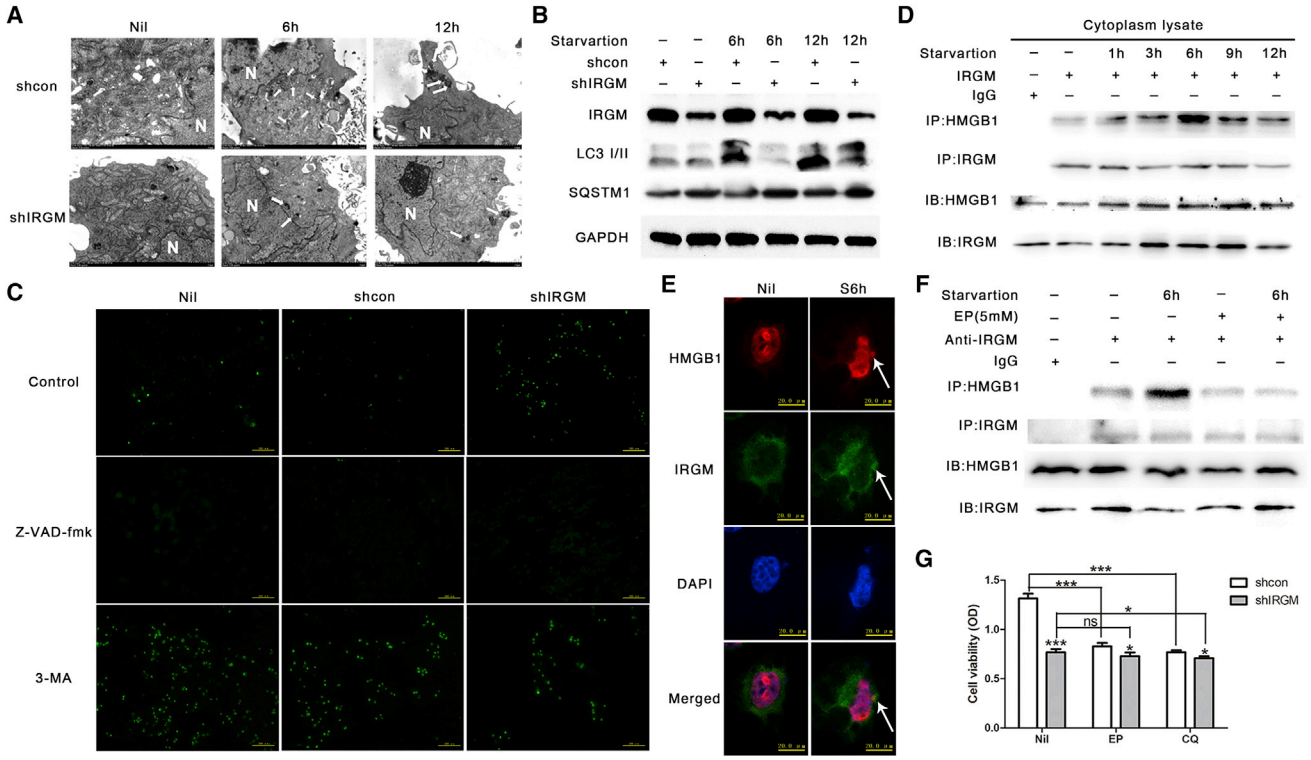

Figure 5. IRGM promotes melanoma cell survival through autophagy by binding HMGB1

A375 cells were treated with control shRNA or IRGM shRNA and cultured in nutrient-deprived medium (starvation) for an additional 6 or 12 h. (A) Transmission electron microscopy was used to detect autophagosomes in A375 cells (white row figured out autophagosomes). (B) The expression of IRGM, LC3 I/II, SQSTM1, and GAPDH by A375 cells was assessed via western blotting. (C) A375 cells were treated with control shRNA or IRGM shRNA and incubated with or without the apoptosis inhibitor Z-VAD-fmk (5 μM) or autophagy inhibitor 3-MA (5 μM) for 24 h. Apoptosis was evaluated via TUNEL staining. (D) A375 cells were cultured in complete medium or serum-deprived low-glucose conditioned medium (starvation) for different time periods (1, 3, 6, 9, or 12 h), and cytoplasmic lysates were obtained. Anti-IRGM monoclonal antibody or non-immune IgG (control) was used to pull down IRGM, and HMGB1 was detected via western blot with an anti-HMGB1 polyclonal antibody. (E) Colocalization of IRGM with HMGB1 in A375 cells after culturing in complete medium or serum-deprived low-glucose conditioned medium (starvation) for 6 h, determined via immunofluorescence staining (red, HMGB1; green, IRGM; blue, nuclei). (F) Non-treated and EP-treated (5 mM) A375 cells (24 h) were cultured in complete or serum-deprived low-glucose conditioned medium (starvation) for 6 h, and total lysates were obtained. Anti-IRGM monoclonal antibody or non-immune IgG (control) was used to pull down IRGM, and HMGB1 was detected via western blot with an anti-HMGB1 polyclonal antibody. (G) A375 cells were treated with control or IRGM shRNA, followed by incubation with EP (5mM) or autophagy inhibitor (CQ, 10 mM) for 24 h. A CCK8 assay was used to evaluate cell viability (means ± SD; *p < 0.05, **p < 0.01, ***p < 0.001).

visualized using the ImmunoCruz mouse ABC staining system (sc-2017; Santa Cruz Biotechnology, Shanghai, China). Evaluation of immunohistochemical scores was not performed for cases with severe melanin diffusion in human melanoma tissue chips. In the 87 melanoma cases obtained from Harbin Medical University Cancer Hospital, diffused melanin was initially removed with oxalic acid and potassium permanganate before IHC staining.

In terms of the immunohistochemical score standard, a brown signal was indicative of positive action. The stain index was determined as a product of intensity and proportion, ranging from 0 to 12. Intensity scores were classified as 0 (negative), 1 (weak), 2 (moderate), or 3 (strong). The proportion, representing the frequency of positive cells, was scored as 0 (<5%), 1 (5%–25%), 2 (26%–50%), 3 (51%–75%), and 4 (>75%). We randomly selected three points in each case and calculated the stain index of each point. The stain index in each case was determined as the average of three points. For statistical analyses, scores of 0–6 were considered as "low expression" and 7–12 as "high expression."

mRNA extraction and real-time PCR

We extracted mRNA from human melanoma paraffin blocks with the RNA pure formalin-fixed, paraffin-embedded (FFPE) kit (CW0535S; CWBIO, Xian, China). Briefly, four to five sections were obtained from blocks for each case (5–10 μm per piece) for mRNA extraction. After removal of paraffin with xylene and ethanol, sections were incubated with protein K. Tissue RNA was extracted and washed with the buffer provided in the kit. All procedures were conducted according to the manufacturer's instructions.

cDNA synthesis was performed using random hexamer primers and a TaqMan reverse transcription kit (04897030001; Roche, Beijing,

China). Samples were subjected to real-time PCR analysis on an ABI StepOne sequence detection system under standard conditions. The sequences of pre-designed primers for human IRGM were as follows: forward primer, 5′-GGACTCTGGCAATGGGATGT-3′; reverse primer, 5′-CCCTCATGTCCTGTGTTTCGA-3′; probe primer, 5′-FAM-ACCTTCATCAGTGCCC-MGB-3′ (Invitrogen, Shanghai, China). The sequences of primers for human IRGM splice isoforms were based on the findings of Singh et al.[9] Expression levels of IRGM and its splice isoforms were normalized with those of actin.

Kaplan-Meier survival analysis and Cox proportional hazards model

According to patients' clinical information, including sex, age, smoking, alcohol use, tumor history, family history, IRGM expression level, and IRGM and its splice isoforms transcript levels, Kaplan-Meier survival analysis HR were performed to search potential common risk factors that promoted melanoma progression and reduced survival within these 78 cases. Furthermore, to verify the independent effects of IRGM or its splice isoform and exclude other elements, a Cox proportional hazards model was established. In this study, IRGM or IRGMb levels were defined as first regression factors to compare patients' survival and calculate the HR value. Statistical significance was defined as $p < 0.05$.

Animals and models

BALB/c nude mice were purchased from HFK Bioscience (Beijing, China). All mice were housed in the animal facility of Harbin Medical University (Harbin, China). Experimental procedures were performed according to the protocols approved by the Institutional Animal Care and Use Committee at the Institute of Genetics and Developmental Biology. Primary melanoma-bearing mice were generated using A375 melanoma cells. Briefly, BALB/c nude mice were injected subcutaneously with 2×10^6 A375 cells in 100 μL of phosphate-buffered saline (PBS). Mice (five/group) were sacrificed on day 30, and tumor sizes and weights were determined. Two independent experiments were conducted, and five mice/group/experiment were included. Furthermore, A375 melanoma cells (1×10^6) were injected into BALB/c nude mice via the tail vein and mouse survival was recorded. Two independent experiments were conducted, and six mice/group/experiment were included.

Cell culture and treatment

A375 cells were purchased from ATCC (Shanghai, China). For experimental purposes, cells were cultured in DMEM supplemented with 10% fetal bovine serum at 37°C in a 5% CO_2 incubator. Cell starvation was induced using serum-deprived, low-glucose conditioned DMEM. The autophagy inhibitors 3-MA and chloroquine (M9281 and C6628; Sigma-Aldrich, USA) were used to block autophagy, and the apoptosis inhibitor Z-VAD-fmk (V116; Sigma-Aldrich, USA) was used to block apoptosis. Nuclear HMGB1 translocation was inhibited with ethyl pyruvate (W245712; Sigma-Aldrich, USA).

GFP-tagged IRGM and negative shRNA plasmids were obtained from Saiye Bioscience (Guangzhou, China). To achieve suppression of IRGM, A375 cells were transfected with IRGM-specific shRNA using Lipofectamine 3000 transfection reagent (L3000015; Thermo Fisher Scientific, USA), according to the manufacturer's instructions.

Cell viability assay

Cell viability was measured using a CCK8 assay (CK04; Dojindo, Beijing, China) according to the manufacturer's protocol. CCK8 solution was added at the final 4 h of the experiment, and absorbance was measured at 490 nm on a microplate reader (Molecular Devices, Sunnyvale, CA, USA).

Annexin V and PI staining

Annexin V staining and PI staining (556547; BD Pharmingen, San Diego, CA, USA) were conducted based on the manufacturer's protocols. Annexin V was labeled with allophycocyanin (APC), and PI was recorded with the same channel of peridinin chlorophyll protein (PerCP). Briefly, cells were washed with cold PBS and resuspended in 1× binding buffer. Annexin V and PI were added to the samples and incubated for 15 min at room temperature, followed by quantification of the respective signals via flow cytometry (BD Accuri C6, BD Biosciences, San Diego, CA, USA).

TUNEL staining

TUNEL-positive cells were detected in keeping with the manufacturer's protocol (11684817910; Roche, Nutley, CA, USA). Briefly, cells were fixed with 4% paraformaldehyde for 15 min at room temperature and permeabilized using 0.25% Triton X-100 in PBS. Next, cells were incubated with TdT reaction buffer and ethynyl dUTP (EdUTP)+TdT enzyme cocktail at 37°C for 1 h, and the TUNEL signal was detected via fluorescence microscopy (Nikon Eclipse 80i, Nikon, Tokyo, Japan).

Immunofluorescence staining

Sections were blocked for 1 h with 10% normal goat serum, 0.3% bovine serum albumin, 0.05% saponin, and 0.3% Triton X-100 in PBS, followed by incubation with primary Abs (anti-Beclin1, 1:200; 3738, Cell Signaling Technology, Shanghai, China; anti-HMGB1, 1:300; ab18256, Abcam, USA; anti-IRGM-1G9, 1:200; AbMart, Shanghai, China) at 4°C. Following overnight incubation, sections were washed with PBS and incubated with fluorescence-labeled secondary Abs (anti-mouse phycoerythrin [PE], 1:400, ab7000; anti-rabbit PE, 1:400, ab7007; anti-mouse fluorescein isothiocyanate [FITC], 1:400, ab6785; anti-rabbit FITC, 1:400, ab6717; Abcam, USA) Next, sections were rinsed in PBS and mounted with gel/mounting medium (MO1, Biomeda, Foster City, CA, USA). Images were captured using fluorescence (Nikon, Tokyo, Japan) and confocal microscopy (Zeiss, Jena, Germany).

Transmission electron microscopy

The cells were dissociated and washed with PBS three times and then soaked in 2% glutaraldehyde for 24 h. The tumor was cut into 1-mm^3 size cubes and also soaked in 2% glutaraldehyde for 24 h. Samples were fixed for 2 h in 1% osmium tetroxide and dehydrated in graded ethanol and embedded in araldite. Ultrathin

sections were cut and stained with uranyl acetate and lead citrate and then observed with a transmission electron microscope (H-765, Hitachi, Tokyo, Japan).

Immunoblotting and CoIP

Total cell lysates were extracted with radioimmunoprecipitation assay (RIPA) cell lysis buffer (P0013C; Beyotime, Shanghai, China) and cytoplasmic lysates with a nucleus and cytoplasm protein kit (P0028; Beyotime, Shanghai, China). IRGM, LC3, P62, HMGB1, Beclin1, and caspase-3 levels in A375 cells were assessed via western blot. The Abs used for western blotting included anti-IRGM monoclonal Ab (1G9; AbMart, Shanghai, China), anti-LC3B Ab (3868; Cell Signaling Technology, Shanghai, China), anti-P62 (39749; Cell Signaling Technology, Shanghai, China), anti-HMGB1 Ab (ab18256; Abcam, USA), anti-Beclin1 Ab (3738; Cell Signaling Technology, Shanghai, China), anti-caspase-3 Ab (AC030; Beyotime, Shanghai, China), anti-cleaved caspases-3 Ab (AC033; Beyotime, Shanghai, China), anti-ACTB (SAB1403520; Sigma, USA), anti-mouse immunoglobulin G (IgG) (horseradish peroxidase [HRP]-linked Ab 7076; Cell Signaling Technology, Shanghai, China), and anti-rabbit IgG (HRP-linked Ab 7074; Cell Signaling Technology, Shanghai, China). For coIP, cell lysates were incubated with anti-IRGM monoclonal Abs at 4°C overnight. The Ab-antigen complex was captured using protein A/G plus agarose (sc-2003; Santa Cruz Biotechnology, USA). HMGB1 and Beclin1 polyclonal Abs were used to measure the binding signal of the complex. Blots were developed with the SuperSignal West Femto Maximum Sensitivity Substrate (Thermo Fisher Scientific, Shanghai, China).

Statistical analysis

Statistical analyses were performed using the SPSS program and GraphPad prism. Patients' survival, HR value, transcript levels, and IHC scores of patient samples were determined as means ± SD (95% confidence interval). All values in the mouse experiments were presented as means ± SD and analyzed using the Mann-Whitney test. Statistical significance was defined as $p < 0.05$.

SUPPLEMENTAL INFORMATION

Supplemental Information can be found online at https://doi.org/10.1016/j.omto.2020.12.005.

ACKNOWLEDGMENTS

This work was supported by grants from the National Natural Science Foundation of China for Young Scholars (no. 81702760 to L.T.); the Natural Science Foundation of Heilongjiang Province for Young Scholars (no. QC2018091 to L.T.); the Science Foundation of Heilongjiang Province Education Department for Young Scholars (no. UNPYSCT-2017052 to L.T.); the National Natural Science Foundation of China (General Program no. 31870894 to H.X.); the National Natural Science Foundation of China (General Program no. 81771305 to H.L.); the National Natural Science Foundation of China (Key Program no. 81430035 to H.L.); and the National Natural Science Foundation of China (no. 81600539 to H.M.).

AUTHOR CONTRIBUTIONS

L.T., X.D., L.Z., Y.Y., R.L., and Z.S. conducted *in vivo* and *in vitro* experiments. H.M. and H.L. designed and performed clinical-related experiments and patient sample collection. L.T. and X.L. analyzed clinical data. R.L. and L.T. designed experiments and wrote the paper. H.X. managed financial support and reviewed the paper. C.P. and B.L. participated in design of experiments.

DECLARATION OF INTERESTS

The authors declare no competing interests.

REFERENCES

1. Schadendorf, D., van Akkooi, A.C.J., Berking, C., Griewank, K.G., Gutzmer, R., Hauschild, A., Stang, A., Roesch, A., and Ugurel, S. (2018). Melanoma. Lancet *392*, 971–984.
2. Poulikakos, P.I., and Rosen, N. (2011). Mutant BRAF melanomas—dependence and resistance. Cancer Cell *19*, 11–15.
3. Franke, V., and van Akkooi, A.C.J. (2019). The extent of surgery for stage III melanoma: how much is appropriate? Lancet Oncol. *20*, e167–e174.
4. Sharma, P., Hu-Lieskovan, S., Wargo, J.A., and Ribas, A. (2017). Primary, adaptive, and acquired resistance to cancer immunotherapy. Cell *168*, 707–723.
5. Robert, C., Grob, J.J., Stroyakovskiy, D., Karaszewska, B., Hauschild, A., Levchenko, E., Chiarion Sileni, V., Schachter, J., Garbe, C., Bondarenko, I., et al. (2019). Five-year outcomes with dabrafenib plus trametinib in metastatic melanoma. N. Engl. J. Med. *381*, 626–636.
6. Deretic, V., and Levine, B. (2018). Autophagy balances inflammation in innate immunity. Autophagy *14*, 243–251.
7. Klionsky, D.J., Abdelmohsen, K., Abe, A., Abedin, M.J., Abeliovich, H., Acevedo Arozena, A., Adachi, H., Adams, C.M., Adams, P.D., Adeli, K., et al. (2016). Guidelines for the use and interpretation of assays for monitoring autophagy (3rd edition). Autophagy *12*, 1–122.
8. Mizushima, N., Levine, B., Cuervo, A.M., and Klionsky, D.J. (2008). Autophagy fights disease through cellular self-digestion. Nature *451*, 1069–1075.
9. Singh, S.B., Ornatowski, W., Vergne, I., Naylor, J., Delgado, M., Roberts, E., Ponpuak, M., Master, S., Pilli, M., White, E., et al. (2010). Human IRGM regulates autophagy and cell-autonomous immunity functions through mitochondria. Nat. Cell Biol. *12*, 1154–1165.
10. He, S., Wang, C., Dong, H., Xia, F., Zhou, H., Jiang, X., Pei, C., Ren, H., Li, H., Li, R., and Xu, H. (2012). Immune-related GTPase M (IRGM1) regulates neuronal autophagy in a mouse model of stroke. Autophagy *8*, 1621–1627.
11. Deretic, V., Saitoh, T., and Akira, S. (2013). Autophagy in infection, inflammation and immunity. Nat. Rev. Immunol. *13*, 722–737.
12. Münz, C. (2009). Enhancing immunity through autophagy. Annu. Rev. Immunol. *27*, 423–449.
13. Wang, F., Xia, X., Yang, C., Shen, J., Mai, J., Kim, H.C., Kirui, D., Kang, Y., Fleming, J.B., Koay, E.J., et al. (2018). *SMAD4* gene mutation renders pancreatic cancer resistance to radiotherapy through promotion of autophagy. Clin. Cancer Res. *24*, 3176–3185.
14. Noman, M.Z., Berchem, G., and Janji, B. (2018). Targeting autophagy blocks melanoma growth by bringing natural killer cells to the tumor battlefield. Autophagy *14*, 730–732.
15. Li, S., Song, Y., Quach, C., Nemecio, D., and Liang, C. (2019). Revisiting the role of autophagy in melanoma. Autophagy *15*, 1843–1844.
16. Dong, H., Tian, L., Li, R., Pei, C., Fu, Y., Dong, X., Xia, F., Wang, C., Li, W., Guo, X., et al. (2015). IFNg-induced Irgm1 promotes tumorigenesis of melanoma via dual regulation of apoptosis and Bif-1-dependent autophagy. Oncogene *34*, 5363–5371.
17. Tian, L., Li, L., Xing, W., Li, R., Pei, C., Dong, X., Fu, Y., Gu, C., Guo, X., Jia, Y., et al. (2015). IRGM1 enhances B16 melanoma cell metastasis through PI3K-Rac1 mediated epithelial mesenchymal transition. Sci. Rep. *5*, 12357.

18. Bekpen, C., Xavier, R.J., and Eichler, E.E. (2010). Human IRGM gene "to be or not to be". Semin. Immunopathol. *32*, 437–444.

19. Pilla-Moffett, D., Barber, M.F., Taylor, G.A., and Coers, J. (2016). Interferon-inducible GTPases in host resistance, inflammation and disease. J. Mol. Biol. *428*, 3495–3513.

20. Chauhan, S., Mandell, M.A., and Deretic, V. (2016). Mechanism of action of the tuberculosis and Crohn disease risk factor IRGM in autophagy. Autophagy *12*, 429–431.

21. Xia, F., Li, R., Wang, C., Yang, S., Tian, L., Dong, H., Pei, C., He, S., Jiang, P., Cheng, H., et al. (2013). IRGM1 regulates oxidized LDL uptake by macrophage via actin-dependent receptor internalization during atherosclerosis. Sci. Rep. *3*, 1867.

22. Rastrelli, M., Tropea, S., Rossi, C.R., and Alaibac, M. (2014). Melanoma: epidemiology, risk factors, pathogenesis, diagnosis and classification. In Vivo *28*, 1005–1011.

23. Chattopadhyay, C., Kim, D.W., Gombos, D.S., Oba, J., Qin, Y., Williams, M.D., Esmaeli, B., Grimm, E.A., Wargo, J.A., Woodman, S.E., and Patel, S.P. (2016). Uveal melanoma: from diagnosis to treatment and the science in between. Cancer *122*, 2299–2312.

24. Farahi, J.M., Fazzari, M., Braunberger, T., Caravaglio, J.V., Kretowicz, A., Wells, K., Dellavalle, R.P., Norris, D., and Alkousakis, T. (2018). Gender differences in melanoma prognostic factors. Dermatol. Online J. *24*, 13030/qt1gs163n8.

25. Poźniak, J., Nsengimana, J., Laye, J.P., O'Shea, S.J., Diaz, J.M.S., Droop, A.P., Filia, A., Harland, M., Davies, J.R., Mell, T., et al. (2019). Genetic and environmental determinants of immune response to cutaneous melanoma. Cancer Res. *79*, 2684–2696.

26. Gandini, S., Masala, G., Palli, D., Cavicchi, B., Saieva, C., Ermini, I., Baldini, F., Gnagnarella, P., and Caini, S. (2018). Alcohol, alcoholic beverages, and melanoma risk: a systematic literature review and dose-response meta-analysis. Eur. J. Nutr. *57*, 2323–2332.

27. Leu, M., Reilly, M., and Czene, K. (2008). Evaluation of bias in familial risk estimates: a study of common cancers using Swedish population-based registers. J. Natl. Cancer Inst. *100*, 1318–1325.

28. Mehto, S., Jena, K.K., Nath, P., Chauhan, S., Kolapalli, S.P., Das, S.K., Sahoo, P.K., Jain, A., Taylor, G.A., and Chauhan, S. (2019). The Crohn's disease risk factor IRGM limits NLRP3 inflammasome activation by impeding its assembly and by mediating its selective autophagy. Mol. Cell *73*, 429–445.e7.

29. Wang, L.L., Jin, X.H., Cai, M.Y., Li, H.G., Chen, J.W., Wang, F.W., Wang, C.Y., Hu, W.W., Liu, F., and Xie, D. (2018). AGBL2 promotes cancer cell growth through IRGM-regulated autophagy and enhanced Aurora A activity in hepatocellular carcinoma. Cancer Lett. *414*, 71–80.

30. Hansen, M.D., Johnsen, I.B., Stiberg, K.A., Sherstova, T., Wakita, T., Richard, G.M., Kandasamy, R.K., Meurs, E.F., and Anthonsen, M.W. (2017). Hepatitis C virus triggers Golgi fragmentation and autophagy through the immunity-related GTPase M. Proc. Natl. Acad. Sci. USA *114*, E3462–E3471.

31. Tang, D., Kang, R., Livesey, K.M., Cheh, C.W., Farkas, A., Loughran, P., Hoppe, G., Bianchi, M.E., Tracey, K.J., Zeh, H.J., 3rd, and Lotze, M.T. (2010). Endogenous HMGB1 regulates autophagy. J. Cell Biol. *190*, 881–892.

32. Tang, D., Kang, R., Cheh, C.W., Livesey, K.M., Liang, X., Schapiro, N.E., Benschop, R., Sparvero, L.J., Amoscato, A.A., Tracey, K.J., et al. (2010). HMGB1 release and redox regulates autophagy and apoptosis in cancer cells. Oncogene *29*, 5299–5310.

33. Zhu, X., Messer, J.S., Wang, Y., Lin, F., Cham, C.M., Chang, J., Billiar, T.R., Lotze, M.T., Boone, D.L., and Chang, E.B. (2015). Cytosolic HMGB1 controls the cellular autophagy/apoptosis checkpoint during inflammation. J. Clin. Invest. *125*, 1098–1110.

34. Liu, B., Gulati, A.S., Cantillana, V., Henry, S.C., Schmidt, E.A., Daniell, X., Grossniklaus, E., Schoenborn, A.A., Sartor, R.B., and Taylor, G.A. (2013). Irgm1-deficient mice exhibit Paneth cell abnormalities and increased susceptibility to acute intestinal inflammation. Am. J. Physiol. Gastrointest. Liver Physiol. *305*, G573–G584.

35. Singh, S.B., Davis, A.S., Taylor, G.A., and Deretic, V. (2006). Human IRGM induces autophagy to eliminate intracellular mycobacteria. Science *313*, 1438–1441.

36. McCarroll, S.A., Huett, A., Kuballa, P., Chilewski, S.D., Landry, A., Goyette, P., Zody, M.C., Hall, J.L., Brant, S.R., Cho, J.H., et al. (2008). Deletion polymorphism upstream of IRGM associated with altered IRGM expression and Crohn's disease. Nat. Genet. *40*, 1107–1112.

37. Chauhan, S., Mandell, M.A., and Deretic, V. (2015). IRGM governs the core autophagy machinery to conduct antimicrobial defense. Mol. Cell *58*, 507–521.

38. Gewirtz, D.A. (2016). The challenge of developing autophagy inhibition as a therapeutic strategy. Cancer Res. *76*, 5610–5614.

39. Chen, D.P., Ning, W.R., Li, X.F., Wei, Y., Lao, X.M., Wang, J.C., Wu, Y., and Zheng, L. (2018). Peritumoral monocytes induce cancer cell autophagy to facilitate the progression of human hepatocellular carcinoma. Autophagy *14*, 1335–1346.

40. Turriani, E., Lázaro, D.F., Ryazanov, S., Leonov, A., Giese, A., Schön, M., Schön, M.P., Griesinger, C., Outeiro, T.F., Arndt-Jovin, D.J., and Becker, D. (2017). Treatment with diphenyl-pyrazole compound anle138b/c reveals that α-synuclein protects melanoma cells from autophagic cell death. Proc. Natl. Acad. Sci. USA *114*, E4971–E4977.

41. Matsuo, T., Daishaku, S., and Sadzuka, Y. (2019). Lactic acid promotes cell survival by blocking autophagy of B16F10 mouse melanoma cells under glucose deprivation and hypoxic conditions. Biol. Pharm. Bull. *42*, 837–839.